Chemical Engineering Journal 144 (2008) 476–482

Contents lists available at ScienceDirect

Chemical Engineering Journal

journal homepage: www.elsevier.com/locate/cej

Modeling and CFD simulation of flow behavior and dispersivity through randomly packed bed reactors

A. Jafari*, P. Zamankhan, S.M. Mousavi, K. Pietarinen

Faculty of Technology, Lappeenranta University of Technology, Lappeenranta, Finland

ARTICLE INFO

Article history:
Received 31 August 2007
Received in revised form 27 June 2008
Accepted 14 July 2008

Keywords:
Modeling
CFD simulation
Flow behavior
Dispersivity
Randomly packed bed reactors

ABSTRACT

Packed bed reactors (PBRs) are multiphase reactors in which gas and liquid phases flow over a solid packing. PBRs find widespread use in petroleum refining, chemical and process industries, pollution abatement and biochemical industries. In this paper numerical study of flow behavior through random packing of non-overlapping spheres in a cylindrical geometry has been carried out using a commercially available computational fluid dynamics package (FLUENT). Dimensionless pressure drop was studied for a fluid through randomly packed bed at different Reynolds numbers based on pore permeability and interstitial fluid velocity. Numerical solution of Navier–Stokes equations in a three-dimensional randomly porous packed bed illustrated that the results are in good agreement with those of reported by Macdonald et al. (1979) in the range of Reynolds number studied. By injection of solute into the system, the dispersivity over a wide range of flow rate has also been investigated. The simulation results have been evaluated by comparing with published experimental results in term of dispersion coefficient. It is shown that the lateral fluid dispersion coefficients in randomly packed beds can be estimated by comparing the concentration profiles of solute obtained by numerical simulations and those derived analytically by solving the macroscopic dispersion equation for the present geometry.

1. Introduction

Packed bed reactors (PBRs) are extensively used in the chemical, environmental and technological processes. In chemical industries, packed beds can be found in diverse applications, being used as reaction, filtration, separation and purification units. Flow hydrodynamics can play a crucial role in determining the performance of such devices. The flow behavior in such systems is very complex due to interactions between fluid and packed particles, particles and column wall, and fluid and column wall. The relative importance of these interactions depends on the operating conditions, ratios of packed particle size to the column diameter, and configuration of the flow system. This will in turn result in different microscopic and macroscopic flow behavior within the packed bed. Despite interesting developments in applications of structured packings in recent years [1], the randomly packed bed is still the state-of-the-art reactor type in these fields.

Computer speed has increased tremendously over the last few years. It becomes interesting, tempting and within acceptable time and cost constraints to simulate packed beds with three-dimensional computational fluid dynamics (CFD), in order to provide insight in flow patterns. CFD is a fast growing technology that can be useful to obtain shorter product–process development cycles, to optimize energy requirements, to optimize existing processes and to efficiently design new products and processes. CFD has allowed promising applications of numerical simulations to the modeling of multiphase flow in packed bed reactors [2–6].

Modeling and simulation are essential tools in design of packed bed reactors, and as the performance requirements of these equipments are growing, it is required that the proposed model be able to define not only spatial distribution of involved fluids but also velocity profiles within the reactor.

CFD applications to simulate fluid flow in a porous matrix are based on the numerical solution of Navier–Stokes equations, with a broad variety of applications ranging from oil basin simulation [7] to modeling of corn seed drying [8]. In all cases, the solution depends on an appropriate geometrical model, mesh definition and the selection of a turbulence model.

There are several models can be used to investigate turbulence flow in porous packed beds. One of the important models is large eddy simulation (LES). LES can be used to calculate flow statistics, which are determined by the larger scales, such as the mean velocity and second-order velocity moments. Indeed, these quantities are often required in practice. Recent advances in physical

* Corresponding author.
E-mail address: ajafari@lut.fi (A. Jafari).

1385-8947/$ – see front matter © 2008 Elsevier B.V. All rights reserved.
doi:10.1016/j.cej.2008.07.033

models, numerical techniques, and computational power together have made LES [9] as a useful tool for investigating turbulence flow regimes in porous beds [10] where the dynamics of larger scales is influenced by the presence of small scales because of nonlinear interactions.

Also the analysis of the dispersivity of fluid flowing through a porous packed bed is important in such systems. Apparently, there are three principal mechanisms that cause dispersion in a granular bed, namely diffusive dispersion which arises from molecular diffusion across the streamlines; mechanical dispersion which arises from stochastic velocity fluctuations of fluid induced by the randomly positions bed particles; and non-mechanical dispersion which arises due to the presence of dead-end pores [11]. Due to the simultaneous presence of these three mechanisms, the dispersivity tensor is complex in nature. The lateral dispersion coefficients, which contribute to the spread of the solute in directions orthogonal to the mean flow, are difficult components of the dispersivity tensor to measure using the solute concentration measuring technique in the bed [12]. Pulsed gradient spin echo NMR method [13], a novel approach, was used to obtain more accurate values for these coefficients. As an adjunct to experiments, simulations may be used to predict detailed information, such as concentration profiles in the direction normal to the mean flow, from which these coefficients may be extracted.

The objective of this work is the modeling and CFD simulation of fluid flow through a bed of non-overlapping spherical particles in a cylindrical geometry as a randomly packed bed. For the pore space with a specified void fraction and a set of fluid physical properties, the Navie–Stokes equations are solved for the velocity and pressure fields in the fluid phase of the pore space by discretization using the control volume method. To investigate the flow hydrodynamics in different regimes, laminar model as well as turbulence models, LES and Reynolds stress model (RSM), were used. The obtained results compared with works described in Refs. [14–17]. The fluid dispersivity was also studied, and the spread of a solute continuously injected to the system was recorded. The method for predicting the lateral dispersion coefficients is similar to the so-called concentration-based methods [18] that utilize solutions of the advection–diffusion equation [18] to calculate the dispersivity from the measured concentration and mean velocity data.

2. Mathematical modeling

2.1. Laminar flow

Since the forces that drive the flow change very slow in time, the steady state flows are often encountered in flow in granular media. The flow is assumed to be horizontal, steady state, incompressible and isothermal. The mathematical description for the flow of a viscous fluid through a three-dimensional granular bed is based on the steady form of the Navier–Stokes and continuity equations [19] for momentum and mass conservation, respectively. By taking the viscosity to be constant, the microscopic equations of motion may be written in the following form:

$$\rho u.\nabla u = -\nabla p + \mu\nabla\cdot\nabla u \quad (1)$$

$$\nabla\cdot u = 0 \quad (2)$$

where ρ, u, p and μ represent density, velocity, pressure, and dynamic viscosity of fluid, respectively. A uniform velocity profile is assumed at the inlet whereas the pressure at the exit is assumed to be fixed to the local atmospheric pressure. In addition, no-slip boundary condition at the entire solid fluid interface is considered.

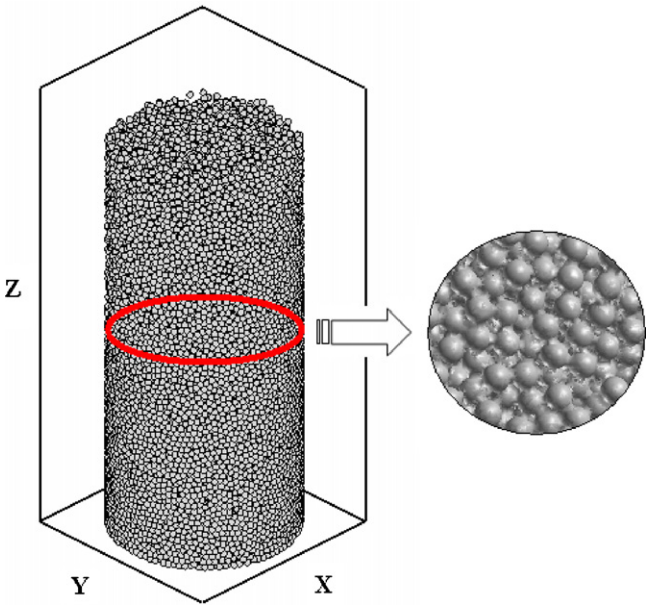

Fig. 1. Particles configuration for the simulations.

2.2. Turbulent flow

In the present work both laminar and turbulence models, LES and RSM, at higher Reynolds numbers were considered. It should be mentioned because performing direct numerical simulation (DNS) in which all scales of the flow are properly resolved for simulating flows in models such as that illustrated in Fig. 1 is not currently feasible due to prohibitive computational requirements, LES and RSM were studied.

Firstly, the application of LES [20], which has the less ambitious goal of describing the larger scales of the flow field through a stationary irregular array of particles, to study of flow regimes was investigated. Using LES the dynamic range of scales to be resolved was reduced by filtering operation performed on the Navier–Stokes equations, so LES generates an approximation in which scales below the filter size are missing. The turbulent energy cascade generates smaller scales and all scales of turbulence are dynamically significant. Given the lack of small scales below a certain size, the correction must be applied via the aforementioned additional terms (known as subgrid stress tensor) in the governing equations of LES. The subgrid scale (sgs) stress tensor describes the effect of the unresolved scales on the larger resolved scales. The replacement of sgs stress by an explicit physical model is required to close equations for the large-scale fields on a grid small enough (but much larger than the Kolmogorov scale) to provide reasonable resolutions. Details of the LES microscopic equations can be found in Ref. [21].

In the following, RSM was applied to investigate of flow behavior in the bed. At high Reynolds numbers, the governing equations for the conservation of mass and momentum are averaged over both time and space [22], and $\overline{u_i'\cdot u_j'}$ has been calculated using differential transport equations. As RSM is a well-known model we avoid to describe the details, however for more information see Ref. [21].

2.3. Dispersion modeling

As stated earlier, at the inlet a constant superficial velocity in z direction in the cylinder, for the solvent is assumed. The geometry is symmetric and a continuous source of solute is located at (0 0 0). The size of the injection port is very small compared to the

diameter of the cylinder to ensure the validity of the point source approximation.

The volume-average form of the transport equation, convection–diffusion equation, was used to calculate the average concentration of fluid phase in granular bed under flow conditions because it is not possible to obtain an exact mathematical description of the motion of each fluid element. The volume average concentration of a solute, $\langle c\rangle$, takes on the form of Fick's law with a constant effective diffusivity coefficient [23]. The dispersive term accounts for the spread of the solute about the mean pulse position due to molecular diffusion and the coupling of interparticle velocity and concentration gradients,

$$\frac{\partial\langle c\rangle}{\partial t} + u.\nabla\langle c\rangle = \nabla.(D.\nabla\langle c\rangle) + S(r,z,t) \tag{3}$$

where D and S refer to the effective diffusivity coefficient, and source term, respectively. The solution of Eq. (3) for cylindrical coordinate system subjected to the initial and boundary conditions given below:

$$\begin{aligned} &\langle c(r,z,0)\rangle = 0\\ &\frac{\partial\langle c\rangle}{\partial\theta} = 0 \text{ (cylinder has symmetry)}\\ &\frac{\partial\langle c\rangle}{\partial r} = 0 \text{ when } r = \pm\frac{d}{2}\\ &\partial\langle c\rangle\big|_{r=0} = \text{finite} \end{aligned} \tag{4}$$

can be expressed in terms of Green's function $F(r, z, r', z', t-\tau)$, which represents the mean concentration at (r,z) at time t resulting from a unit source at (r', z') at time τ, as follows [24]:

$$\langle c(r,z,t)\rangle = \int_{-\frac{d}{2}}^{\frac{d}{2}}\int_{-\infty}^{\infty}\int_{0}^{t}[F(r,z,r',z',t-\tau)\cdot\delta(r',z',t)\cdot d\tau\cdot dr'\cdot dz'] \tag{5}$$

where d is cylinder diameter. The Green's function satisfies

$$\frac{\partial F}{\partial t} + \frac{u_{z,0}}{\phi}\cdot\frac{\partial F}{\partial z} = D_{rr}\cdot\frac{1}{r}\cdot\frac{\partial}{\partial r}\cdot\left(r\cdot\frac{\partial F}{\partial r}\right) + D_{zz}\cdot\frac{\partial^2 F}{\partial z^2} \tag{6}$$

Here $u_{z,0}$ and ϕ are superficial fluid velocity and porosity, respectively. Also $F(r, z, r', z', 0) = \delta(r-r')\cdot\delta(z-z')$ and the boundary conditions for Eq. (6) are given by

$$\begin{aligned} &\frac{\partial F}{\partial r} = 0 \text{ when } r = \pm\frac{d}{2}\\ &\left.\frac{\partial F}{\partial r}\right|_{r=0} = \text{finite} \end{aligned} \tag{7}$$

In order to obtain Eq. (6) it is assumed that the coefficients of diffusivity are constant and the overall mean fluid velocities in the y and z-directions are small. By applying the transformation $\xi = z - z' - (t-\tau)\cdot V_{z,0}/\phi$ to Eq. (6), it can be reduced to:

$$\frac{\partial F}{\partial t} = D_{rr}\cdot\frac{1}{r}\cdot\frac{\partial}{\partial r}\cdot\left(r\cdot\frac{\partial F}{\partial r}\right) + D_{zz}\cdot\frac{\partial^2 F}{\partial\xi^2} \tag{8}$$

Using separation of variables, the following expression for the Green's function can be obtained [24]:

$$F = \frac{1}{\pi\cdot d^2\cdot\sqrt{4\cdot\pi\cdot D_{zz}\cdot(t-\tau)}}\frac{-\left(\xi-\xi'\right)^2}{e^{4\cdot D_{zz}\cdot(t-z)}} \times\left[1+\sum_{\alpha}e^{-D_{rr}\cdot\alpha^2\cdot(t-\tau)}\cdot\frac{J_0(\alpha\cdot r)\cdot J_0(\alpha\cdot r')}{J_0^2\left(\alpha.\frac{d}{2}\right)}\right] \tag{9}$$

where J is Bessel function, and α shows its roots. To obtain the lateral dispersion in a granular bed, the Green's function may be obtained by neglecting diffusion in the z-direction as compared with convection and by taking into account that

$$\lim_{D_{zz}\to 0}\frac{\frac{-\left(\xi-\xi'\right)^2}{e^{4\cdot D_{zz}\cdot(t-\tau)}}}{\sqrt{4\cdot\pi\cdot D_{zz}\cdot(t-\tau)}} = \delta\left[z-z'-(t-\tau)\cdot u_{z,0}/\phi\right] \tag{10}$$

That is

$$F = \frac{\delta[z-z'-(t-\tau)\cdot u_{z,0}/\phi]}{\pi\cdot d^2} \times\left[1+\sum_{\alpha}e^{-D_{rr}.\alpha^2.(t-\tau)}\cdot\frac{J_0(\alpha\cdot r)\cdot J_0(\alpha\cdot r')}{J_0^2(\alpha.d/2)}\right] \tag{11}$$

Substituting the expression for F from Eq. (11) into Eq. (5) the concentration resulting from a continuous point source of solute with strength q located at (0 0 0) may be given as

$$\begin{aligned}\langle c(z,r,t)\rangle = \int_{-\frac{d}{2}}^{\frac{d}{2}}\int_{-\infty}^{\infty}\int_{0}^{t}&\left[\frac{\delta[z-z'-(t-\tau)\cdot u_{z,0}/\phi]}{\pi\cdot d^2}\right]\\ &\times\left[1+\sum_{\alpha}e^{-D_{rr}.\alpha^2.(t-\tau)}\cdot\frac{J_0(\alpha\cdot r)\cdot J_0(\alpha\cdot r')}{J_0^2(\alpha.d/2)}\right]\\ &\times q\cdot\delta[z'+\frac{1}{2}L_z]\cdot\delta(r').d\tau\cdot dr'\cdot dz'\end{aligned} \tag{12}$$

Evaluating the integral in Eq. (12), the expression for the solute concentration becomes:

$$c(r,z) = \frac{4\cdot q\cdot\phi}{u_{z,0}\cdot\pi\cdot d^2}\times\left[1+\sum_{\alpha}e^{\frac{-D_{rr}\cdot\alpha^2\cdot\phi\cdot(1/2L_z+z)}{u_{z,0}}}\cdot\frac{J_0(\alpha\cdot r)}{J_0^2(\alpha.d/2)}\right] \tag{13}$$

where L_z is the length of packed bed. Following Cussler [18], diffusion coefficients D_{rr} in cylindrical geometry may be replaced by the dispersion coefficients $E_z(r) = u_{z,0}^2 d^2/4\pi^2\phi D_{rr}$, Eq. (13) becomes:

$$c(r,z) = \frac{4\cdot q\cdot\phi}{u_{z,0}\cdot\pi\cdot d^2}\times\left[1+\sum_{\alpha}e^{\frac{-\alpha^2\cdot u_{z,0}\cdot d^2\cdot(1/2L_z+z)}{4\pi^2 E_z(r)}}\cdot\frac{J_0(\alpha\cdot r)}{J_0^2(\alpha.d/2)}\right] \tag{14}$$

Note that the dispersion coefficients depend inversely on the diffusion coefficients.

3. Implementation of numerical method

Fig. 1 illustrates non-overlapping uniform size spheres randomly distributed within a cylinder. During this research, using Matlab software and a C++ code applied to the commercial grid-generation tool, GAMBIT 2.2 (Fluent Inc.), a defined number of randomly positioned non-overlapping spheres in a specified three-dimensional domain was developed. A code obtained by Matlab uses random number generator which carefully positions specific number of non-overlapping spheres in a particular domain. The C++ code generates a journal file for preprocessor, which creates three-dimensional geometry. The input parameters defined by user are the number of spheres, radius of spheres and dimensions of the geometry. Nevertheless more details about this method can be found in Ref. [25].

In this work smooth and roughened wall cylinders were studied. As shown in Fig. 2(a) the walls are smooth and, therefore, regions of higher velocity are expected to exist near the walls due to the presence of large pores in the wall region. As illustrated in Fig. 2(b) the walls are roughened by adding spherical caps to create a system with a reasonably large spread of pore sizes in the wall region.

The spherical particles as well as the cylinders are impermeable to the continuous phase. Different number and diameter

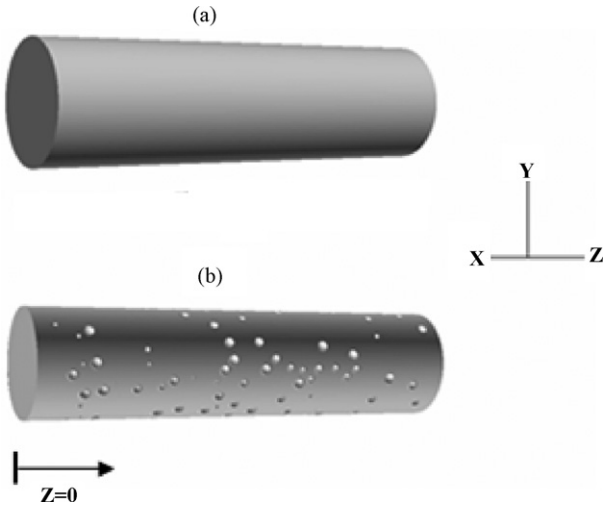

Fig. 2. Two different used geometries with (a) smooth walls and (b) rough walls. The length and diameter of cylinders are 21 and 6 cm, respectively.

of particles are tested to obtain different porosity. Also longer cylinders were investigated to show that porosity has more effect on dimensionless pressure drop compare to length of the tubes.

Eqs. (1) and (2) are solved numerically for the pressure and velocity fields using the finite volume method with the pressure correction algorithm SIMPLE [26]. In dealing with the fixed pressure boundary at the exit the pressure corrections are set to zero at the nodes just inside the exit boundary. The Power-Law scheme is used for the discretization of convective terms. To divide the pore space into discrete control volumes more than 2×10^6, three-dimensional tetrahedral computational cells were used. In addition, roughly 5×10^5 wall triangular elements and more than 10^4 at the inlet and exit were used. It is very important to use adequate number of computational cells while numerically solving the governing equations over the solution domain. The grid is shown in Fig. 3. Using under-relaxation factors 0.5 and 0.7 for the pressure and velocities, respectively a reasonable rate of convergence was achieved. The convergence was considered to be achieved when the conservation equations of mass and momentum were satisfied, which was considered to have occurred when the normalized residuals became smaller than 5×10^{-5}. The normalization factors used for the mass and momentum were the maximum residual values after the first few iterations.

4. Results and discussion

Numerical results for the roughened cylinder are shown in Fig. 4. The dimensionless pressure drop predicted by the soft cylinder is lower than that of roughened geometry. A comparison between the first model and the correlations proposed by [14–17] implies that there should be large pores in the wall region through which the main portion of fluid flowing from inlet to exit [27]. However, comparison between studies of Soleymani et al. [27] and the results reported here represents that the cubic geometry has problem of channeling and fluid flows more to the corners. So it seems that choosing a cylindrical geometry for investigation of flow through a porous media is more accurate. Also most of industrial geometries are cylinder.

Fig. 4 illustrates the plots of dimensionless pressure drop $(-\mathrm{d}p/\mathrm{d}z)K/\mu V_\mathrm{f}\phi$, versus the Reynolds number based on pore permeability and interstitial fluid velocity, $Re_K = \rho V_\mathrm{f}\sqrt{K/\phi}/\mu$, as suggested by Kececioglu and Jiang [15]. In these definitions, $-\mathrm{d}p/\mathrm{d}z$, K and V_f represent pressure drop, permeability, and interstitial fluid velocity magnitude, respectively. As illustrated in Fig. 4(a), a Darcy regime can be observed for numerical results over a range of Reynolds number for which the dimensionless pressure drop is equal to a constant. Using this part of the simulations and Darcy's law, the porous bed permeability was determined as shown in Fig. 5.

A large number of efforts have been expended on determining K. The most widely used expression to calculate permeability is Kozeny–Carman's correlation. The following semi-empirical expression has been found to accurately represent many experimental data.

$$K = \frac{d_\mathrm{p}^2\phi^3}{36k(1-\phi)^2} \tag{15}$$

where k is experimentally determined and is a measure of tortuosity of the fluid path thorough the pores, and for smooth spherical particles is equal to 5 [28]. In this equation d_p represents the particle diameter. According to Fig. 5 the Kozeny–Carman relation breaks down in high porosity regimes. Martys et al. [29] also have shown that Eq. (15) in the high porosity regimes is not suitable, and they suggested their relation:

$$K = 2[1-(\phi-\phi^c)](\phi-\phi^c)^f/s^2 \tag{16}$$

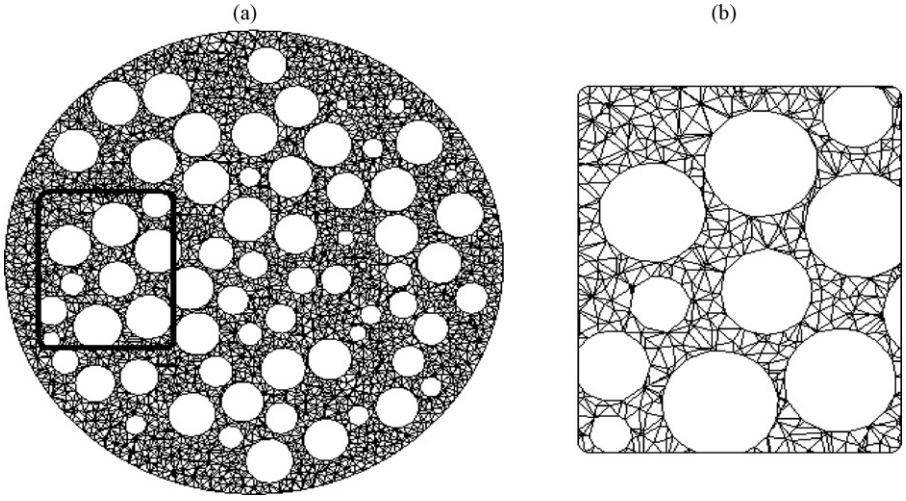

Fig. 3. (a) The mesh view on a plane located at $z = 0.1$ m. (b) To obtain better visualization the highlighted part in (a) is magnified.

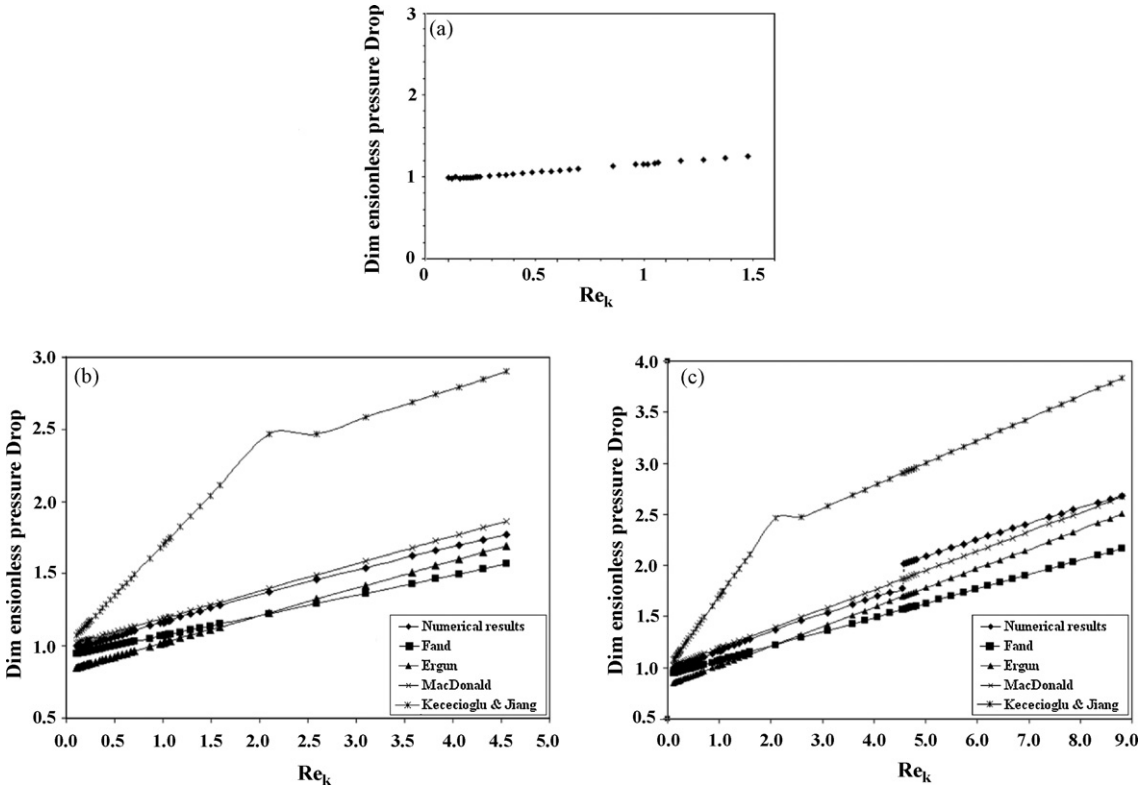

Fig. 4. Plot of dimensionless pressure drop vs. Re_K for the roughened cylinder. (a) Darcy flow based on numerical results, (b) Darcy and Forchheimer regimes and (c) Darcy and two post-Darcy regimes.

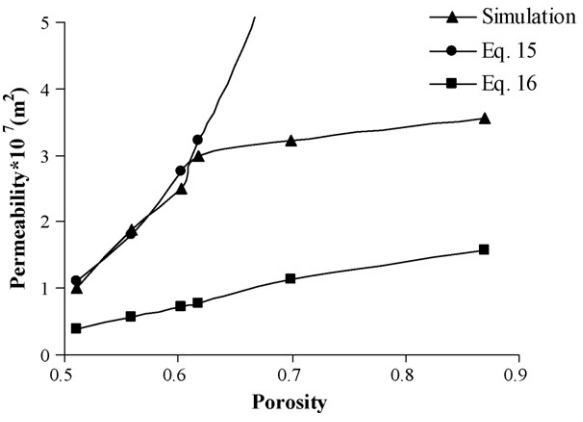

Fig. 5. Comparison of simulation results of permeability calculation at different porosity with Eqs. (15) and (16).

where $\phi^c = 0.055$ and $f \approx 4.2$. Since $1/s$ represents a length scale associated with a typical pore size, the power low term in the above expression accounts for the tortuosity. As can be seen in Fig. 5 the formula proposed by Martys et al. [29] cannot predict the permeability well.

Fig. 4(b) illustrates the post-Darcy regime. The change in the slope as shown in Fig. 4(c) indicates the transition to the turbulent regime. The transition criteria from laminar to turbulent flow for flow through porous media have not been yet defined. Authors proved numerically that the flow regime demarcation varies with permeability [21]. In addition, Kececioglu and Jiang [15] from their experimental work showed that particle diameter has effect on flow regime. A comparison between the numerical results and the values obtained from the correlations proposed by other researchers, which are listed in Table 1 implies that the numerical results are in good agreement with those of Macdonald et al. [16]. There is a slightly difference in slopes when transition to the second post-Darcy regime occurs, but the maximum error is less than 10%. The differences between the calculated dimensionless pressure drop and those in [15] could be attributed to the inaccuracy of the

Table 1
Correlations for dimensionless pressure drop vs. Reynolds number based on pore permeability and interstitial fluid velocity for flow through porous bed [15]

	Forchheimer flow	Turbulent flow
Ergun [17]	$\frac{P'K}{\mu v} = 0.83 + 0.19\hat{R}e_K; \quad 0.08 < \hat{R}e_K < 196$	
Macdonald et al. [16]	$\frac{P'K}{\mu v} = 1 + 0.19\hat{R}e_K; \quad 0.003 < \hat{R}e_K < 32.7$	
Fand et al. [14]	$\frac{P'K}{\mu v} = 0.93 + 0.14\hat{R}e_K; \quad 0.57(\pm 0.06) < \hat{R}e_K < 9(\pm 0.6)$	$\frac{P'K}{\mu v} = 1.14 + 0.12\hat{R}e_K; \quad \hat{R}e_K > 13.5$
Kececioglu and Jiang [15]	$\frac{P'K}{\mu v} = 1(\pm 0.15) + 0.7(\pm 0.15)\hat{R}e_K$	$\frac{P'K}{\mu\ v} = 1.9(\pm 0.1) + 0.22(\pm 0.04)\hat{R}e_K$

Table 2
Effect of LES and RSM models on dimensionless pressure drop at constant Reynolds number and porosity

Numerical results	Macdonald et al. [16]	Fand et al. [14]	Ergun [17]	Kececioglu and Jiang [15]
1.929 (LES)	1.916	1.605	1.746	2.961
2.272 (RSM)	1.916	1.605	1.746	2.961

Table 3
Effect of mesh on dimensionless pressure drop

Grid	#1	#2	#3
Number of tetrahedral elements	5×10^5	2×10^6	6×10^6
Number of nodes	$\approx 2 \times 10^5$	4×10^5	9×10^5
Numerical results (dimensionless pressure drop)	1.56	1.929	1.920

experimental procedures, or to some other reason such as misinterpretation of the results using simplified theories.

The values of dimensionless pressure drop at the transition regime from laminar to turbulence are shown in Table 2. Comparison of numerical results obtained by LES and RSM shows that LES model with using Smagorinsky for sgs model have a better agreement with results of other researchers specially Macdonald et al. [16]. Turbulence in the mentioned system is a controversial issue, indeed three-dimensional fluctuations occur on length scales that range from very small pores with the size of fraction of particle diameter to the scales much larger than particle diameter and on a correspondingly broad range of time scales. Hence, it is necessary to describe fluid flow in a wide range of length and time scales. Modeling of this system requires a mathematically rigorous modeling methodology capable of predicting coupling behaviors from the very small scales through full-scale system.

A grid independency check has been conducted to ensure that the results from the runs are not grid dependent. To do this test, three different grids have been chosen. Their details and obtained numerical results with using LES model and every grid are shown in Table 3. The results appear to be grid independent. There was no significant variation in the dimensionless pressure drop resulted by the grid with 2×10^6 elements and those obtained from the fine grid, so the grid with 2×10^6 elements was selected for all calculations.

Fig. 6 illustrates the color image of velocity field within the porous matrix. The velocity magnitude was evaluated in the plane $(z-y)$ passing through the center of the bed and the plane $(x-y)$ at $z = 5$ cm. Contours of velocity magnitude indicate that average velocity in the near side wall region but not on the wall is higher than in the center region of porous medium. Fluid layers close to the walls tend to move faster resulting in a flattened velocity profile.

In a porous bed relaminarization could occur after diverging sections as well as turbulence enhancement after converging sections. In this light, LES is a potentially powerful tool for providing detailed and accurate solution of flow in a porous packed bed at high Reynolds numbers. In addition our calculations with the Navier–Stokes equations indicate that the laminar model should be valid for low Reynolds numbers and also for a limited range of high Reynolds numbers.

To test the roughened cylinder further the lateral fluid dispersivities were calculated for the first post-Darcy regime at an axial position within the bed. As mentioned earlier, it is of interest to obtain the evolution of the mass fraction profile of a solute injected into the bed of particles filled with solvent flowing due to dispersion in the axial direction. The molecular diffusivity of the solute in the solvent is assumed to be a constant. In Eq. (14) all of parameters except dispersion coefficient are known. To link between CFD and dispersion modeling it was assumed that concentration profiles calculated by Eq. (14) and that obtained from simulation at each Peclet number which is defined as

$$\mathrm{Pe} = \frac{u \times L_z}{D_{rr}} \tag{17}$$

should be equal to each other. To satisfy this assumption a desired dispersion coefficient is needed. Mathematica software (version 5.2) was applied to implement trial and error method to obtain this dispersion coefficient. Fig. 7, as an example, shows the solute mass fraction profile at Pe = 7.5. To validate this method, several dispersion coefficients were determined at different Peclet numbers as shown in Fig. 8. According to this figure the estimated dispersion coefficients (simulation results) are in agreement with the results reported in [13], therefore the theoretical equation derived by authors, Eq. (14), is able to predict concentration profile in porous beds.

The fluid dispersivity in the bed is essentially isotropic. As shown in Fig. 9, when the solute moves through the bed the peak of mass fraction profile (which is close to a Gaussian) decays in the streamwise direction indicating the mixing of the solute and the solvent. In order to provide a deeper investigation of the subject, the solute

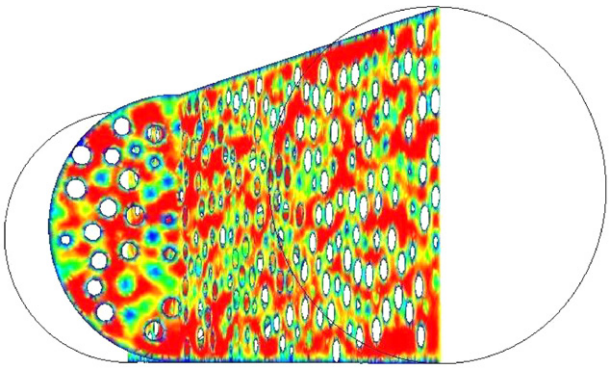

Fig. 6. Contour plot of velocity field in the porous bed. The figure is color coded by velocity magnitude, where the red is for the highest and blue represents the lowest. (For interpretation of the references to color in this figure legend, the reader is referred to the web version of the article.)

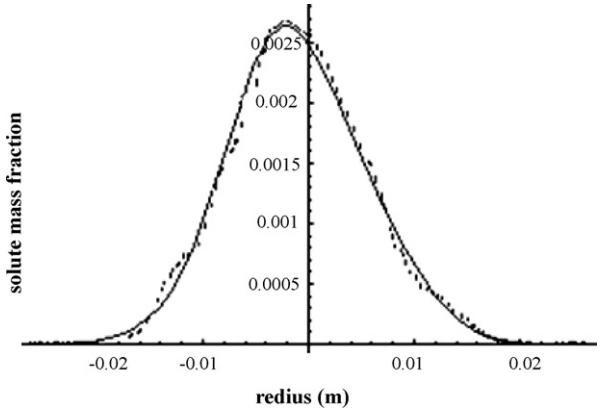

Fig. 7. The mass fraction profile of solute at $z = 0.05$ m which $u_{z,0} = 0.012$ m/s, $\phi = 0.602$, $q = 0.019 \times 10^{-7}$ kg/s, Pe = 7.5 and the solute source is located at $z = r = 0$. The dashed line represents the simulation results and the solid line shows the calculated solute mass fraction using Eq. (14).

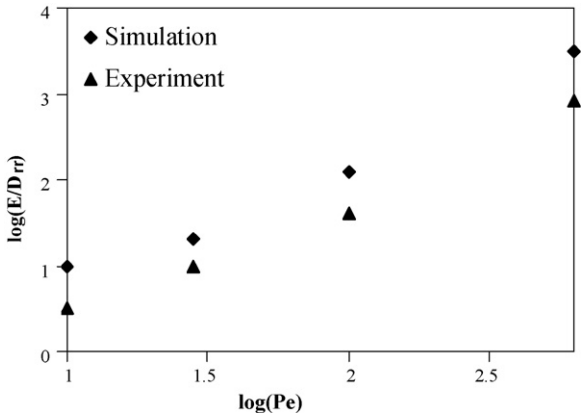

Fig. 8. Log of longitudinal dispersion coefficient normalized by effective diffusivity coefficient as a function of Log of Peclet number.

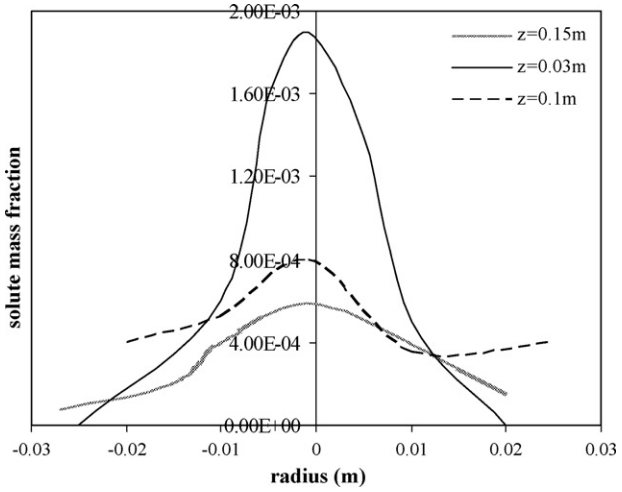

Fig. 9. The solute mass fraction profiles at different distance from the solute source.

transport could be estimated by calculating the individual trajectories of a large number of non-interacting tracer particles. This detailed study will be the subject of the future paper.

5. Conclusion

Numerical study of flow through randomly packing of non-overlapping spheres in cylindrical geometries (smooth and rough wall) is investigated. Assuming rough walls, the simulation results for pressure drop across the bed agreed well with the correlation of Macdonald et al. [16] for the range of actual flow Reynolds studied here. Further analysis is needed of the details of the mechanism of turbulent generation, which will be examined in a future study. Results of smooth geometry confirm that there should be large pores in the wall region through which the main portion of fluid flowing from inlet to exit. Simulations were done using a model based on the Navier–Stokes equations, including inertial terms but without a turbulence model, for range of conditions studied in the second post-Darcy ("turbulent") flow regime to examine the fluid flow in a granular bed. For the first post-Darcy (Forchheimer) flow regime, the calculated results for the dispersion coefficients in the roughened geometry were found to be in agreement with those of Seymour and Callaghan [13] and also results of cubic geometry reported by Soleymani et al. [27].

References

[1] H.P.A. Calis, J. Nijenhuis, B.C. Paikert, F.M. Dautzenberg, C.M. van den Bleek, CFD modelling and experimental validation of pressure drop and flow profile in a novel structured catalytic reactor packing, Chemical Engineering Science 56 (4) (2001) 1713–1720.
[2] F.H. Yin, C.G. Sun, A. Afacan, K. Nandakumar, K.T. Chuang, CFD modeling of mass-transfer processes in randomly packed distillation columns, Industrial & Engineering Chemistry Research 39 (5) (2000) 1369–1380.
[3] A.G. Dixon, M. Nijemeisland, CFD as a design tool for fixed-bed reactors, Industrial & Engineering Chemistry Research 40 (2001) 5246–5254.
[4] Y. Jiang, M.R. Khadilkar, M.H. Al-Dahhan, M.P. Dudukovic, CFD modeling of multiphase flow distribution in catalytic packed bed reactors: scale down issues, Catalysis Today 66 (2–4) (2001) 209–218.
[5] Y. Jiang, M.R. Khadilkar, M.H. Al-Dahhan, M.P. Dudukovic, CFD of multiphase flow in packed-bed reactors. I. k-fluid modeling issues, AIChE Journal 48 (2002) 701–715.
[6] Y. Jiang, M.R. Khadilkar, M.H. Al-Dahhan, M.P. Dudukovic, CFD of multiphase flow in packed-bed reactors. II. Results and applications, AIChE Journal 48 (2002) 716–730.
[7] M. Allen, F. Furtado, Computational methods in porous-media flows, in: J.P. du Pleiss (Ed.), Advances in Fluid Mechanics: Fluid Transport in Porous Media, Computational Mechanics Publications, Southampton, UK, 1997, pp. 255–302.
[8] M. Prakash, Ö.F. Turan, Y. Li, G.R. Thorpe, CFD Modeling of natural convection heat and mass transfer in hygroscopic porous media, Drying Technology 18 (2000) 2175–2201.
[9] S. Ghosal, P. Moin, The basic equations of the large eddy simulation of turbulent flows in complex geometry, Computation Journal of Physics 118 (1995) 24–37.
[10] F. Kuwahara, T. Yamane, A. Nakayama, Large eddy simulation of turbulent flow in porous media, International Communications in Heat and Mass Transfer 33 (4) (2006) 411–418.
[11] J.R.F. Guedes de Carvalho, J.M.P.Q. Delgado, Overall map and correlation of dispersion data for flow through granular packed beds, Chemical Engineering Science 60 (2) (2005) 365–375.
[12] N. Han, J. Bhakta, R.G. Carbonell, Longitudinal and lateral dispersion in packed beds: effect of column length and particle size distribution, AIChE Journal 31 (1985) 277–287.
[13] J.D. Seymour, P.T. Callaghan, Generalized approach to NMR analysis of flow and dispersion in porous media, AIChE Journal 43 (1997) 2096–2110.
[14] R.M. Fand, B.Y. Kim, A.C.C. Lam, R.T. Phan, Resistance to the flow of fluids through simple and complex porous media whose matrices are composed of randomly packed spheres, Journal of Fluids Engineering 109 (1987) 268–273.
[15] I. Kececioglu, Y. Jiang, Flow through porous media of packed spheres saturated with water, Journal of Fluid Engineering 116 (1994) 164–170.
[16] I.F. Macdonald, M.S. EI-Sayed, A.L. Dullien, Flow through porous media—the Ergun equation revisited, Industrial & Engineering Chemistry Fundamentals 18 (3) (1979) 199–207.
[17] S. Ergun, Fluid flow through packed columns, Chemical Engineering Progress 48 (1952) 89–94.
[18] E.L. Cussler, Diffusion Mass Transfer in Fluid Systems, 2nd ed., Cambridge University Press, New York, 1997.
[19] H. Schlichting, Boundary-Layer Theory, McGraw-Hill, New York, 1979.
[20] P. Sagaut, Large Eddy Simulation for Incompressible Flows, 2nd ed., Springer, Berlin, 2002.
[21] A. Jafari, P. Zamankhan, S.M. Musavi, K. Piteraninen, P. Sarkomaa, Investigation of flow dynamics in porous media using computer simulation, in: The 2006 European Simulation and Modeling Conference Toulouse, France, 2006.
[22] M.R. Raupach, R.H. Shaw, Averaging procedures for flow within vegetation canopies, Boundary Layer Meteorology 22 (1982) 79–90.
[23] J. Bear, Dynamics of Fluids in Porous Media, Dover Publications, Inc, Mineola, New York, 1988.
[24] H.S. Carslaw, J.C. Jaeger, Conduction of Heat in Solid, 2nd ed., Oxford University Press, Briston, England, 1959.
[25] P. Zamankhan, T. Tynjala, W. Polashenski Jr., P. Zamankhan, P. Sarkomaa, Stress fluctuations in continuously sheared dense granular materials, Physical Review E 60 (6) (1999) 7149–7156.
[26] Fluent, 6.2 Users Guide Inc.: Lebanon, 2005.
[27] A. Soleymani, E. Takasuo, P. Zamankhan, W. Polashenski Jr., Fluid flow and lateral fluid dispersion in bounded granular beds, in: ASME International Mechanical Engineering Congress, Proceedings of the IMECE02, 2002.
[28] P.C. Carman, Fluid Flow Through a Granular Bed, vol. 15, Transactions of Institute of Chemical Engineers, London, 1937, pp. 150–156.
[29] N.S. Martys, S. Torquato, D.P. Bentz, Universal scaling of fluid permeability for sphere packings, Physical Review E 50 (1994) 403–408.